Surface depletion and electrical transport model of AlInP-passivated GaAs nanowires

2013 Semicond. Sci. Technol. 28 105026

(http://iopscience.iop.org/0268-1242/28/10/105026)

Semicond. Sci. Technol. **28** (2013) 105026 (8pp) doi:10.1088/0268-1242/28/10/105026

Surface depletion and electrical transport model of AlInP-passivated GaAs nanowires

A C E Chia[1], M Tirado[2], F Thouin[3], R Leonelli[3], D Comedi[4,5] and R R LaPierre[1]

[1] Department of Engineering Physics, Centre for Emerging Device Technologies, McMaster University, Hamilton, ON L8S 4L7, Canada
[2] Laboratorio de Nanomateriales y de Propiedades Dieléctricas, Departamento de Física, FACET, Universidad Nacional de Tucumán, Avenida Independencia 1800, 4000 Tucumán, Argentina
[3] Department of Physics, Université de Montréal, Montreal, QC H3C 3J7, Canada
[4] Laboratorio de Física del Sólido, Departamento de Física, FACET, Universidad Nacional de Tucumán, Avenida Independencia 1800, 4000 Tucumán, Argentina
[5] Consejo Nacional de Investigaciones Científicas y Técnicas (CONICET), Argentina

E-mail: lapierr@mcmaster.ca

Received 1 June 2013, in final form 8 August 2013
Published 10 September 2013
Online at stacks.iop.org/SST/28/105026

Abstract
Fabrication, current–voltage characterization and analytical modeling of an AlInP-passivated GaAs nanowire (NW) ensemble device are presented. During fabrication, sonication was used as a novel and crucial step to ensure effective contacting of the NWs. Current–voltage characteristics of the passivated NW devices were fitted using an analytical surface depletion and transport model which improves upon established models by implementing a non-uniform density of GaAs surface states and including a NW diameter distribution. Scanning electron microscopy, capacitance–voltage characterization and secondary ion mass spectrometry were used to fix key parameters in the model. A 55% decrease in surface state density was achieved upon passivation, corresponding to an impressive four order of magnitude increase in the effective carrier concentration of the NWs. Moreover, the thickest NWs in the ensemble were found to dictate the device characteristics, which is a behavior that should be common to all ensemble NW devices with a distribution in radius. As final confirmation of effective passivation, time-resolved photoluminescence measurements showed a 25 × improvement in carrier lifetime upon passivation. The fabrication and passivation methods can be easily implemented into future optoelectronic applications.

(Some figures may appear in colour only in the online journal)

1. Introduction

III–V semiconductor nanowires (NWs) have been studied extensively due to the promise of novel optoelectronic applications. These applications capitalize on the small diameter of NWs which allow for quantum confinement, novel heterostructures and the growth of NWs on lattice-mismatched substrates [1]. However, these small NW diameters also serve to magnify harmful surface effects such as carrier depletion and surface recombination. These surface effects have been shown experimentally to significantly reduce device performance [2]. Recent numerical modeling of radial GaAs NW solar cells has shown that surface depletion and recombination are the primary factors limiting NW solar cell efficiency [3]. This stresses the need for surface passivation to reduce the density of surface states.

While successful surface passivation of Si NWs has been reported frequently [4], surface passivation of GaAs NWs is less common. Chemical surface passivation of GaAs NWs using $(NH_4)_2S$ has demonstrated an order of magnitude

decrease in surface state density [5] and was subsequently implemented into a GaAs NW ensemble solar cell to improve the relative conversion efficiency by 19% [6]. Unfortunately, this type of sulfur passivation layer is unstable in oxygen, thus casting doubt on its long-term viability.

Surface passivation of GaAs NWs using various III–V materials have also been explored. By growing InGaP shells radially onto GaAs cores, photoluminescence (PL) intensity was found to increase by three orders of magnitude [7]. Perhaps the most common III–V passivation material to date has been AlGaAs with a GaAs capping layer. AlGaAs passivation of GaAs NW sidewalls has shown a 20× improvement in PL intensity [8], an order of magnitude decrease in surface recombination velocity using time-resolved photoluminescence (TRPL) [9], and an 82% decrease in surface state density using time-resolved terahertz spectroscopy [10].

In this work, GaAs NW surfaces were passivated with a lattice-matched AlInP shell. Due to its wide bandgap and low refractive index, AlInP lends itself well to optoelectronic applications and is already currently used as a window layer in solar cells [11] and a cladding layer in lasers and LEDs [12]. The performance of AlInP as a passivation layer was assessed in this work by fabricating ensemble NW devices and comparing the current–voltage (*I–V*) characteristics between AlInP-passivated GaAs NW devices and unpassivated GaAs NW reference devices. TRPL measurements were also conducted to compare carrier lifetimes between passivated and unpassivated GaAs NWs. With the exception of a sulfur passivated GaAs NW ensemble solar cell [6], all aforementioned reports have been based on optical characterization of single NWs to confirm passivation. As such, this is one of the first reports of surface passivation demonstrated by electrical characterization of a NW ensemble device with a III–V passivating shell.

2. Experimental details

The radial GaAs-AlInP heterostructure NWs were grown by the Au-assisted vapor–liquid–solid (VLS) mechanism using a gas source molecular beam epitaxy (MBE) system. In preparation for growth, an n-type GaAs (1 1 1)B substrate with a silicon doping density of (1–5)×10^{18} cm^{-3} was pre-cleaned by a 20 min UV ozone, followed by a 30 s buffered HF bath and finally a 10 min rinse in deionized (DI) water. The substrate was then transferred into an electron-beam evaporation system where 1 nm of Au was deposited onto the substrate to serve as the seed particle for VLS growth. Finally, the substrate was placed in the MBE system where it underwent several degassing and plasma cleaning steps (described elsewhere [13]) in preparation for NW growth. The NWs were then grown, starting with the n-type GaAs core. The GaAs core was grown at a high growth temperature of 600 °C for 30 min with a V/III flux ratio of 2.3 and a two-dimensional equivalent growth rate of 0.5 μm h^{-1}. The GaAs core segment was also doped with Te to achieve a nominal doping density of 1×10^{18} cm^{-3} as calibrated by previous thin film growths. Finally, the undoped, nominally lattice-matched $Al_{0.52}In_{0.48}P$ shell was grown at a lower temperature of 500 °C and a higher V/III flux ratio of 3.5 to promote shell growth, while keeping the growth rate and duration the same as that of the core. An unpassivated reference sample was also grown using the same conditions but without the AlInP shell growth.

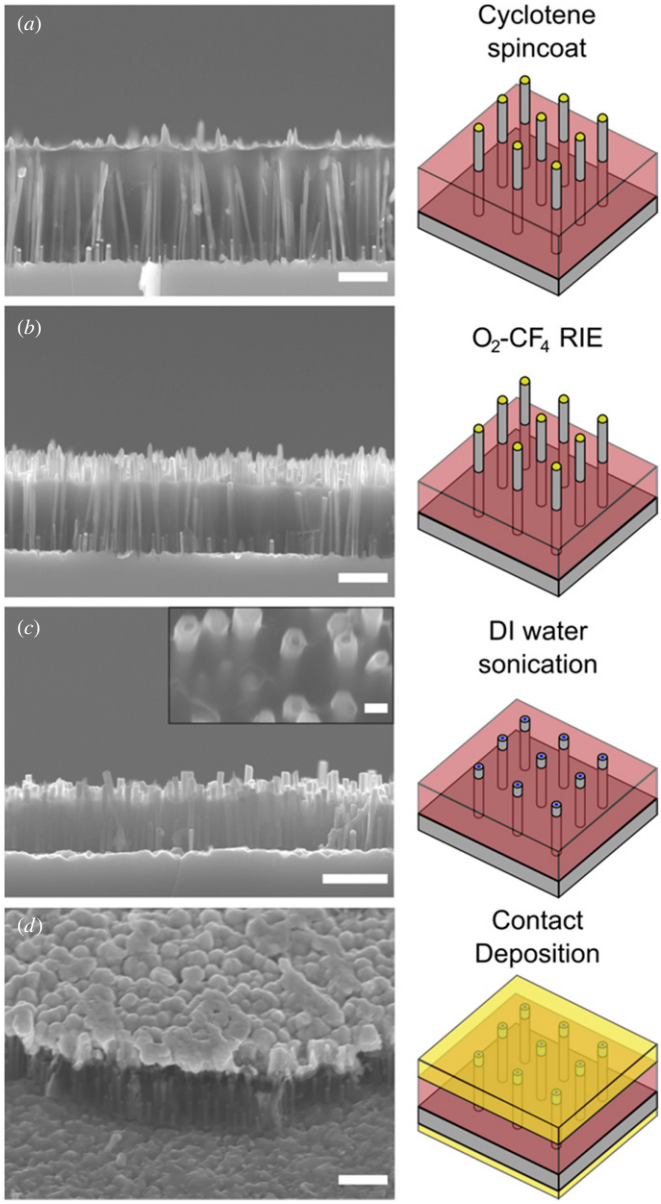

Figure 1. Tilted and side-view SEM images and schematics of the NW ensemble (*a*) after spin-coating with the cyclotene mixture (1 μm scale bar), (*b*) after RIE (1 μm scale bar), (*c*) after DI water sonication (1 μm scale bar). Inset: tilted view (100 nm scale bar), and (*d*) after contact deposition and annealing (1 μm scale bar).

A JEOL JSM-7000F scanning electron microscope (SEM) was used to characterize the as-grown NW ensemble, while a JEOL 2010F high resolution transmission electron microscope (TEM) was used to characterize individual NWs removed from the substrate by sonication.

After characterization by electron microscopy, an ensemble NW resistor device was fabricated using a series of processing steps outlined schematically in figures 1(*a*)–(*d*). First, a 3:1 volume mixture of cyclotene 3022–35 to T1100

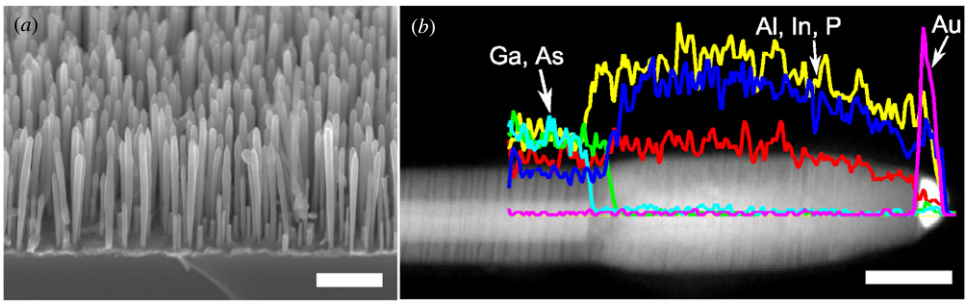

Figure 2. (*a*) 45° tilted SEM image of the as-grown NW ensemble (1 μm scale bar). (*b*) HAADF image of an individual NW. Superimposed EDX linescans indicate the presence of Ga (green) and As (cyan) in the core; Al (red), In (blue) and P (yellow) in the shell and top axial segment; and the Au (purple) seed particle at the top of the NW. The scale bar is 50 nm.

thinner was spin-coated onto the passivated and unpassivated NW ensemble samples to act as a planarizing material to achieve the structure shown schematically in figure 1(*a*). Cyclotene was selected due to its high thermal stability, low porosity, low surface roughness and high electrical resistivity as reported previously [14]. Next, the cyclotene layer was back-etched to a height of ∼1 μm by reactive ion etching (RIE) in a 1:1 mixture (by flow rate) of O_2 and CF_4 as shown schematically in figure 1(*b*). Thereafter, the samples were sonicated in DI water for 60 min using a Branson 1510 ultrasonic cleaner. This was used as a novel method to remove the tops of the NWs that were exposed above the polymer film. This method also removed the AlInP segment covering the top of the NWs to expose the GaAs core for electrical contacting and achieve complete planarization of the NW array as shown schematically in figure 1(*c*). Finally, an array of 0.5 mm^2 top contact pads composed of 50 nm Ni, 100 nm Ge and 650 nm Au, and a bottom substrate contact composed of 25 nm Ni, 50 nm Ge and 120 nm Au were deposited by electron beam evaporation (as shown schematically in figure 1(*d*)) followed by subsequent annealing at 400 °C in N_2 for 30 s to alloy the contacts to the GaAs. The details of these processing steps are reported thoroughly elsewhere [14].

Upon completion of device fabrication, *I–V* characteristics of the passivated and unpassivated samples were measured across the length of NWs (between top and bottom contacts, as shown schematically in figure 3(*a*)) using a two-point probe system with a Keithley 2400 sourcemeter. In this work, positive bias corresponds to the situation whereby the top of the NWs are held at a potential, +V, while the bottom of the substrate is tied to ground. Capacitance–voltage (*C–V*) characteristics were also measured between top and bottom contacts on unpassivated NW devices using a Hewlett Packard HP4192A analyzer with 0.01 V modulation voltage at 1 kHz. The sample was connected to the instrument by means of the HP 16047 C Test Fixture. Dynamic secondary ion mass spectrometry (SIMS) was performed on the unpassivated NW sample to ascertain the doping density in the NWs. The details of this SIMS analysis has been reported elsewhere [15].

Finally, TRPL was used to confirm surface passivation. Laser excitation was at a wavelength of 780 nm, repetition rate of 76.1 MHz, pulse duration of ∼2 ps, and power of 250 μW. Measurements were performed at 14 K in a closed-cycle, exchange-gas cryostat. The PL signal was dispersed with a 50 cm focal length spectrometer with 600 g mm^{-1} grating. Detection was performed with a charge-coupled device for time-integrated PLspectra, or a silicon avalanche photodiode (Si-APD) for time-resolved (TRPL) spectra. Time-correlated single photon counting electronics were from Picoquant.

3. Results

SEM characterization of as-grown NWs in figure 2(*a*) showed a dense array of vertical NWs with heights varying between 1 μm and 2.5 μm and a NW density of approximately 2×10^9 cm^{-2}. The radius of unpassivated NWs varied from 10–36 nm, while that of the passivated NWs varied from 15–80 nm due to the additional thickness of the AlInP shell. High angle annular dark field (HAADF) TEM imaging of sonicated NWs in figure 2(*b*) showed a 'spear' morphology near the NW top. The contrast stripes across the NW diameter are stacking faults, commonly observed in NWs and reported previously [16, 17]. The energy dispersive x-ray spectroscopy (EDX) linescan showed that the NW top underneath the Au particle (the 'spear head') is composed only of AlInP, while the NW base contains both the GaAs core and the AlInP shell. The detection of Al, In and P in the base region of the NW in the EDX linescan come from the shell in front of and behind the GaAs core. By examining the Z contrast in HAADF imaging, it is clear that the NW is composed of a GaAs core denoted by the bright high-Z contrast, and a surrounding AlInP shell denoted by the dark low-Z contrast. The $Al_xIn_{1-x}P$ shells were found by EDX to have an average composition of $x = 0.52$ with a standard deviation of 0.03, confirming a lattice-match to the GaAs core. The HAADF imaging indicated a typical AlInP shell thickness of 5 nm near the base of the NWs to 45 nm near the top of the NWs, thus giving reason for the reverse tapering observed in figure 2(*a*). HAADF imaging confirmed that the GaAs core was encapsulated by AlInP throughout its entire length.

A comparison of the respective SEM images and schematics in figure 1 show that the desired structures were achieved at each processing step. *I–V* measurements described below indicated that the AlInP shells conducted negligible current. Hence, removal of the axial, 'spear head' section of AlInP (shown in figure 2(*b*)) was imperative to successfully contact the conductive GaAs cores instead of the insulating AlInP. This was accomplished by the sonication procedure.

Table 1. Parameter values used in model.

Variable	Description	Value	Reference/source
a	NW radius	Figure 5(b)	SEM
N_D^+	Donor concentration in NW	9.1×10^{17} cm^{-3}	SIMS
D_{it}	Density of interface states along GaAs NW surface	Figure 4	C–V
L	Length of NWs	900 nm	SEM
A_{NWs}	Area of the tops of the NWs under a contact pad	1.05×10^{-4} cm^{-2}	SEM
A_{pad}	Area of a contact pad	5.03×10^{-3} cm^{-2}	SEM
$N_{D,sub}$	Donor concentration in the substrate	2.5×10^{18} cm^{-3}	Known
$\varepsilon_c/\varepsilon_0$	Cyclotene relative permittivity	2.65	Known
$\varepsilon/\varepsilon_0$	GaAs relative permittivity	12.9	19
N_C	Effective density of states in conduction band	4.7×10^{17} cm^{-3}	19
μ_n	Electron mobility	3000 cm^{-2} V^{-1} s^{-1}	19
μ_p	Hole mobility	150 cm^{-2} V^{-1} s^{-1}	19
τ_p	Excess hole carrier lifetime in the substrate	1 ns	24
τ_n	Excess electron carrier lifetime in the NWs	1 μs	24
ψ_{CNL}	Charge neutrality level	0.53 eV	19
R_s	Parasitic series resistance in the measurement apparatus	3 Ω	I–V
r_c	Specific contact resistivity	10^{-6} Ω cm^{-2}	22
R_{lk}	NW leakage resistance	1.2 GΩ	20
n	Ideality factor	3	23

In previous reports [14], sonication was proven useful only in achieving planarization and removing the Au catalysts at the top of the NWs. While that is certainly achieved here as shown by the planar NW ensemble in figure 1(c), sonication has also proven to be useful in removing the AlInP 'spear head' as shown clearly by the exposed GaAs cores in the inset of figure 1(c). Due to its mechanical nature, this technique can be broadly applied to all NW heterostructures composed of other materials. From figure 1(c), the length of the NWs in the device were found to equal 900 nm as tabulated in table 1.

Figure 3(b) shows I–V curves of both passivated and unpassivated NWs using the corresponding color-coded two-point probe configurations found in figure 3(a). Firstly, it must be noted that a parasitic series resistance of 3Ω exists within the measurement apparatus, which was added to the subsequent model as a series resistance, R_s. I–V characteristics measured laterally across contact A (green triangles) and vertically across the GaAs substrate and film alone (without NWs) at contact C (blue triangles) showed linear behavior with a resistance equal to the parasitic series resistance. This indicated a relatively small contribution of the film, substrate and top contact to the overall series resistance. Secondly, the I–V curve was found to be weakly rectifying due to factors discussed in section 4. Due to the weak rectification and the treatment of the reverse bias behavior in previous reports [14], this report solely focuses on the forward bias characteristics displayed in figure 3(b). Thirdly, a comparison of the I–V characteristics measured across passivated NWs (red triangles) showed a two order of magnitude increase in current and four order of magnitude decrease in high-bias resistance compared to unpassivated NWs (black triangles). The passivated NWs showed a current limited by R_s at high bias. Additionally, further I–V measurements of passivated NWs (not shown) with the axial AlInP sections left intact were found to draw two orders of magnitude less current than the unpassivated NWs, thus confirming that conduction occurred almost exclusively within the GaAs cores. As such, the increase in current flow upon the addition of the AlInP shell signifies successful passivation. Results of the characterization using C–V and TRPL are deferred to discussions below.

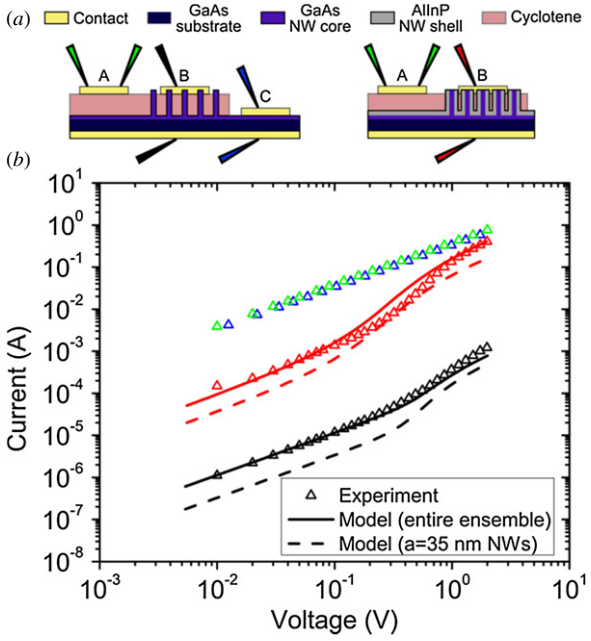

Figure 3. (a) Schematic of the three different top contacts deposited on unpassivated (left) and passivated (right) NW devices with varying two-point probe configurations. (b) Current–voltage measurements across a single contact pad (green), the substrate alone (blue), passivated NWs (red) and unpassivated NWs (black). Model-generated I–V curves (solid lines) of the entire ensemble and that from the upper 1% of NW diameters (dashed lines). The colors of the curves correspond with the probe colors in (a).

4. Model

To fully examine the extent of surface passivation, the I–V characteristics were fit using a combination of two models: a surface depletion model and a transport model. The surface

depletion model was taken mostly from previously published work by Chia *et al* [18], but does not assume complete ionization of donor impurities and contains modifications to include a density of surface states which is nonuniform across the bandgap. This surface depletion model determined the variation in electric potential as a function of radius in the NW and the resultant effective carrier concentrations needed for the subsequent transport model. The transport model enabled the NW ensemble to be modeled using an equivalent circuit from which the *I–V* fits were generated.

4.1. Surface depletion model

For a cylindrical NW, Poisson's equation can be reduced to an ordinary differential equation in r, the radial distance:

$$\frac{\partial^2\psi}{\partial r^2} + \frac{1}{r}\frac{\partial\psi}{\partial r} = -\frac{\rho}{\varepsilon} \tag{1}$$

where ρ is the net bulk charge density, ψ is the electric potential and ε is the permittivity of GaAs. As per previous reports [18], the $\psi(r)$ is defined to be the potential difference between the radially changing intrinsic level, E_i, and the Fermi level, E_f, where the potential is set at zero.

4.1.1. Partially depleted regime. As per Chia *et al* [18], the potential in the NW is given by:

$$\psi(r) = \begin{cases} \psi_0 & \text{for} \quad 0 < r < r_q \\ \psi_0 + \dfrac{qN_D^+ r_q^2}{2\varepsilon}\left[-\dfrac{r^2}{2r_q^2} + \ln\left(\dfrac{r}{r_q}\right) + \dfrac{1}{2}\right] & \text{for} \quad r_q < r < a \end{cases} \tag{2}$$

where q is the elementary charge, N_D^+ is the ionized donor doping density, r_q is the radius of the quasi-neutral core region of the NW, ψ_0 is the potential along the center axis of the NW and a is the radius of the GaAs core. To fully express $\psi(r)$, ψ_0 and r_q must be determined.

ψ_0 can be determined using Fermi–Dirac statistics which states that $n = N_D^+$ at the NW center:

$$\frac{2}{\sqrt{\pi}} N_c F_{1/2}(\eta_{F0}) = N_D^+ \quad \text{where} \quad \eta_{F0} = \frac{q\psi_0 - E_g/2}{kT} \tag{3}$$

where $F_{1/2}(\eta)$ is the Fermi–Dirac integral, N_c is the effective density of states in the conduction band, E_g is the bandgap energy, k is the Boltzmann constant, and T is the temperature.

r_q can be determined by invoking charge neutrality which states:

$$\pi\left(a^2 - r_q^2\right)qN_D^+ + 2\pi aQ_{\text{it}} = 0 \tag{4}$$

where Q_{it} is the surface charge density. This states that r_q is uniquely expressed in terms of Q_{it} for a NW of known a and N_D^+.

Along the NW sidewalls [18]:

$$Q_{\text{it}} = -q^2 \int_0^{(\psi_s+\Delta)} D_{\text{it}}(V)\,\mathrm{d}V \tag{5}$$

where D_{it} is the density of interface states at the GaAs NW surface, $\psi_s \equiv \psi(r = a)$ is the surface potential, and $\Delta \equiv \frac{E_g}{2q} - \psi_{\text{CNL}}$ where ψ_{CNL} is the charge neutrality level (CNL). For GaAs, $\psi_{\text{CNL}} = 0.53\text{V}$ measured from the valence band edge [19] and thus, $\Delta = 0.18\text{V}$. It is clear that Q_{it} is uniquely determined by ψ_s for a NW of known $D_{\text{it}}(V)$. In turn, ψ_s at the surface of the NW ($r = a$) is given by equation (2) to yield:

$$\psi_s = \frac{qN_D^+ r_q^2}{2\varepsilon}\left[-\frac{a^2}{2r_q^2} + \ln\left(\frac{a}{r_q}\right) + \frac{1}{2}\right] + \psi_0. \tag{6}$$

In summary, given a NW with known N_D^+, a and $D_{\text{it}}(V)$, $\psi(r)$ can be determined transcendentally from equations (2) to (6).

4.1.2. Fully depleted regime. In the previous analysis, r_q cannot be solved for all a values. For a specific set of N_D^+ and $D_{\text{it}}(V)$ values, there exists a critical radius, a_{crit}, below which the entire NW is depleted. To find a_{crit}, equation (4) must be solved for a in the limit as r_q approaches zero. For $a > a_{\text{crit}}$, the NW is in the partially depleted regime, allowing application of the previous analysis. However, for $a < a_{\text{crit}}$, the NW is in the fully depleted regime ($r_q = 0$) and is treated as follows.

As per Chia *et al* [18], the potential in a fully depleted NW is given by:

$$\psi(r) = \psi_0 - \frac{qN_D^+}{4\varepsilon}r^2 \quad \text{for } 0 < r < a. \tag{7}$$

ψ_0 can be found by invoking charge neutrality, examining the surface charge. This yields equations (4) and (5) again, but with $r_q = 0$. These equations can be combined to give an expression for Q_{it} which is a transcendental equation in ψ_s given a NW with known N_D^+, a and $D_{\text{it}}(V)$:

$$-\frac{aqN_D^+}{2} = -q^2 \int_0^{(\psi_s+\Delta)} D_{\text{it}}(V)\,\mathrm{d}V. \tag{8}$$

ψ_0 can subsequently be determined easily from equation (7):

$$\psi_0 = \psi_s + \frac{qN_D^+}{4\varepsilon}a^2. \tag{9}$$

With ψ_0 determined, a complete expression for $\psi(r)$ can be given as per equation (7).

4.2. Capacitance model

In the previous analysis, it remains to determine $D_{\text{it}}(V)$. $D_{\text{it}}(V)$ for the unpassivated NWs was estimated from measured *C–V* characteristics. The differential form of the surface charge density can be stated as:

$$\mathrm{d}Q_{\text{it}} = -q^2 D_{\text{it}}(V)\,\mathrm{d}V \tag{10}$$

where V is an applied bias and D_{it} is the density of states at the GaAs surface. This equation qualitatively states that at some applied bias, V, an infinitesimal change in the surface charge density, $\mathrm{d}Q_{\text{it}}$, is equal to $D_{\text{it}}(V)$ multiplied by the infinitesimal change in energy range (of filled surface states), $q\mathrm{d}V$, multiplied by the elementary charge, q. From equation (5), $D_{\text{it}}(V)$ is related to the capacitance across the NWs, C_{NWs}, according to [19]:

$$C_{\text{NWs}}(V) = \frac{\mathrm{d}Q}{\mathrm{d}V} = A_{\text{NWs}}q^2 D_{\text{it}}(V) \tag{11}$$

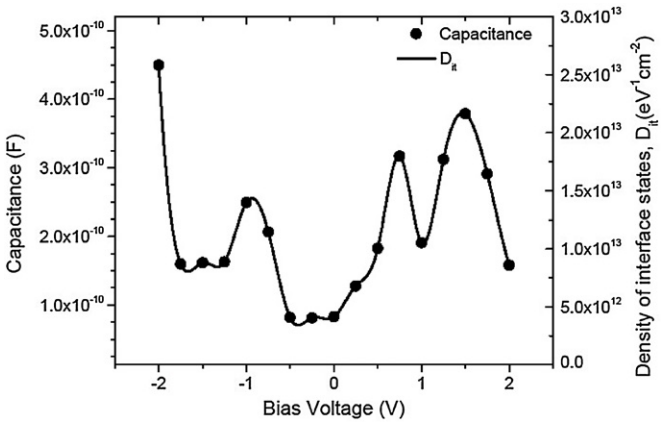

Figure 4. 1 kHz-modulated *C–V* data (black circles, left axis) and interpolated D_{it} (V) (solid line, right axis) for unpassivated NWs.

where A_{NWs} is the area of the tops of the NWs under a contact pad. The total capacitance between top and bottom contacts is estimated as:

$$C_{tot}(V) = C_{NWs}(V) + C_c = C_{NWs} + \frac{\varepsilon_c(A_{pad} - A_{NWs})}{L} \quad (12)$$

where C_c is the capacitance across the cyclotene, ε is the permittivity of the cyclotene and A_{pad} is the area of the contact pad. C_c was found to be 12.8 pF. Combining equation (12) with equation (11) allows $D_{it}(V)$ to be calculated. In this analysis, we assume that the *C–V* characteristic is dominated by surface (interface) states at the NW-contact interface, and that this surface state density is similar to that on the NW sidewalls.

Using the previous analysis, the measured *C–V* data in figure 4 (left axis) was interpolated to yield $D_{it}(V)$, which is plotted in figure 4 as the black solid line. For the passivated sample, we assumed that the surface passivation reduced $D_{it}(V)$ by a constant factor across the bias range (i.e., for all V). This is consistent with previous reports which assume a uniform surface state distribution density that is reduced by a constant factor upon passivation. For example, in [10], a constant D_{it} with a reduction by a constant factor of 82% was assumed.

4.3. Transport model

To relate model generated $\psi(r)$ functions to carrier transport, one must first use the Fermi–Dirac integral to determine the free electron and hole densities, $n(r)$ and $p(r)$, respectively [18]. The effective free carrier densities in a particular nanowire NW_i can then be found by integrating and subsequently averaging $n(r)$ and $p(r)$ across the radius a_i of NW_i:

$$n_{eff,i} = \frac{1}{\pi a_i^2}\int_0^{a_i} n(r)2\pi r\,dr \quad (13)$$

$$p_{eff,i} = \frac{1}{\pi a_i^2}\int_0^{a_i} p(r)2\pi r\,dr. \quad (14)$$

With these effective carrier densities calculated numerically, all necessary carrier transport equations can be solved. The NW ensemble device was modeled with an equivalent circuit shown in figure 5(*a*). Each parallel branch in

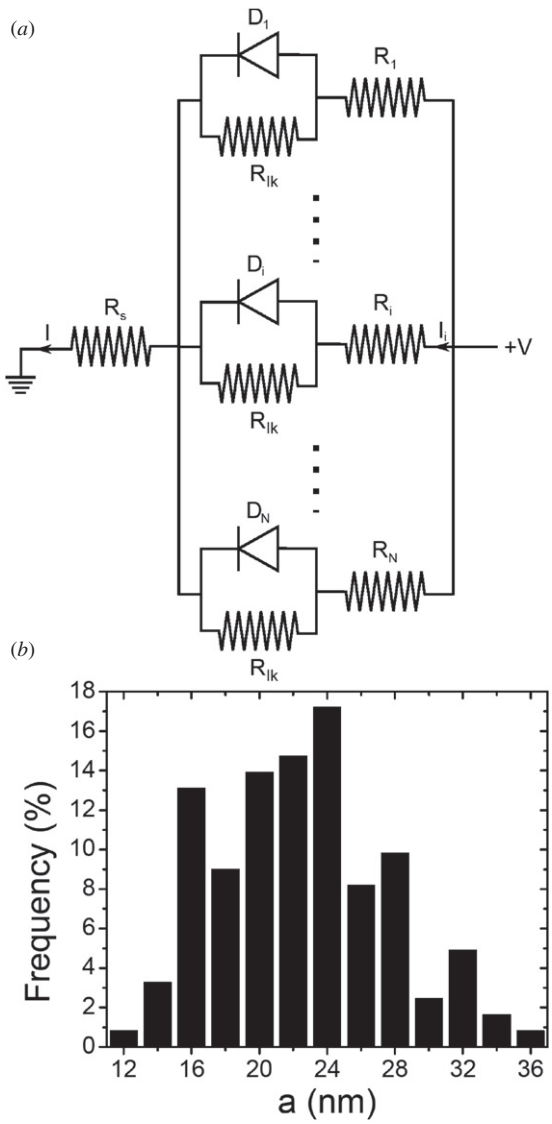

Figure 5. (*a*) Equivalent circuit diagram of the ensemble device. The left side represents the bottom contact, while the right side represents the top contact. (*b*) Radius distribution of all contacted GaAs cores.

figure 5(*a*) represents a single NW and is composed of a diode D_i, series resistor R_i and identical leakage resistor R_{lk}.

The diode, D_i, arises due to the surface depletion of each NW_i. As will be shown in the subsequent discussion, surface depletion of the NWs results in effective electron concentrations of approximately 10^{13} and 10^{17} cm^{-3} for even the thickest unpassivated and passivated NWs, respectively. For the thinner NWs that comprise the rest of the ensemble, the effective electron concentration is even lower, even reaching intrinsic levels at some radii. This makes the NWs resemble a lightly doped or even intrinsic GaAs material. Since the NWs are in contact with a highly doped substrate with a carrier concentration of (1–5) $\times$ 10^{18} cm^{-3}, electrons will diffuse from the substrate into the NWs, thus establishing a potential barrier. In effect, this creates a 'n-n$^+$' junction at the NW–substrate interface of each NW_i which can be modeled by a diode, D_i. As confirmed experimentally, D_i is expected to give weak rectification relative to a p–n junction. Assuming low

injection, it can be easily shown that the reverse saturation current for D_i is given in general by [19]:

$$I_{0,i} = \pi a_i^2 q \left(\frac{D_p p_{\text{sub}}}{L_p} + \frac{D_n n_{\text{eff},i}}{L_n} \right) \tag{15}$$

where D_p, L_p and p_{sub} are the diffusion coefficient, diffusion length and carrier concentration for holes in the n-doped substrate while D_n, L_n and $n_{\text{eff},i}$ are the diffusion coefficient, diffusion length and effective carrier concentration for electrons in NW_i.

The series resistance, R_i, represents the resistance of NW_i as determined by the surface depletion model. Under low injection, the conductance of a shell of radius r and infinitesimal thickness $\text{d}r$ is given by $\text{d}G_i = q[\mu_e n(r) + \mu_p p(r)]2\pi r\,\text{d}r/L$ where μ_e is the electron mobility, μ_p is the hole mobility and L is the length of the NW. Thus, the conductance of NW_i can be found by integrating with respect to radius to yield a NW resistance of:

$$R_i = (G_i)^{-1} = \left(\frac{\sigma_{\text{eff},i} \pi a_i^2}{L} \right)^{-1} \tag{16}$$

where $\sigma_{\text{eff},i} = q(\mu_e n_{\text{eff},i} + \mu_p p_{\text{eff},i})$. Taking into consideration the specific contact resistance, r_c, finally yields:

$$R_i = \left(\frac{\sigma_{\text{eff},i} \pi a_i^2}{L} \right)^{-1} + \frac{r_c}{\pi a_i^2}. \tag{17}$$

Finally, R_{lk} in figure 5(*a*) represents a possible leakage path for current to bypass the NWs. Current leakage has been previously observed in single NW *I–V* measurements [20] with a possible source being surface charge hopping [21].

Standard circuit analysis of figure 5(*a*) shows that the current flowing through a single NW, I_i, and the voltage drop across the parallel branches, V', can be related by the transcendental equation:

$$I_i(V') = I_{0,i} \left[\exp\left(\frac{V' - I_i R_i}{n V_t} \right) - 1 \right] + \frac{V' - I_i R_i}{R_{\text{lk}}} \tag{18}$$

where n is the ideality factor, $V_t = kT/q$ is the thermal voltage and $V = V' + IR_s$ is the applied bias. To fit the experimental *I–V* data, I_i is summed over the entire NW radius distribution under the contact pad $\left(I = \sum_{i=1}^{N} I_i\right)$, thus yielding the total current measured from a contact pad. The NW radius distribution in figure 5(*b*) was determined from SEM measurements.

5. Analysis and discussion

Table 1 summarizes the model parameters. As described earlier, SEM characterization was used to measure the distribution in NW radius. SIMS was used to measure the dopant concentration from which the ionized dopant concentration was determined as $N_D^+ = (9.1 \pm 0.7) \times 10^{17}$ cm^{-3}. $N_D^+ = 9.8 \times 10^{17}$ cm^{-3} was found to provide the best fit to the data and falls within the measurement uncertainty. The value of r_c was taken for GaAs contacted with Ni–Ge–Au [22] and was found to have a negligible contribution compared to the parasitic series resistance. The ideality factor, n, in equation (18) was found to have a value of 3, consistent with the large ideality factors as high as 4.52 previously observed in p–n junction NWs [23]. To fit the unpassivated data at low bias, R_{lk} was set to 1.2 GΩ. With these and the remaining parameters [19, 24] in table 1, a good fit to the *I–V* measurements was obtained as shown in figure 3(*b*). Most importantly, the passivated NW *I–V* data were fit with a reduction in D_{it} of 55%. At zero bias, this represents a reduction from $D_{\text{it}} = 4.2 \times 10^{12}$ cm^{-2} eV^{-1} for unpassivated NWs to $D_{\text{it}} = 1.9 \times 10^{12}$ cm^{-2} eV^{-1} in passivated NWs, which rivals the performance of previous AlGaAs and $(NH_4)_2S$ passivation results [5, 10].

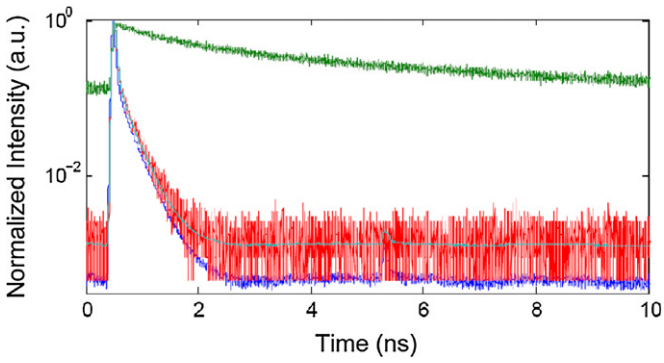

Figure 6. TRPL decay curves comparing passivated NWs (green) with unpassivated NWs (red). The blue curve shows the system response, while the cyan curve is a fit to the unpassivated NW PL spectrum.

Figure 3(*b*) also shows the model *I–V* curve for passivated NWs (red dashed line) and unpassivated NWs (black dashed line) using only the GaAs NWs with radii varying between $a = 34$ nm and $a = 35$ nm. This range represents the top 1% of the NW ensemble radius distribution. The similarity in magnitude between the current drawn by the entire ensemble and the current drawn by the thickest 1% of the NW ensemble shows that the current is dominated by the $a \sim 35$ nm NWs due to their low resistance relative to smaller radius NWs. Upon examination of $\psi(r)$ for both unpassivated and passivated NWs, it was found that the unpassivated $a = 35$ nm NWs were fully depleted with the Fermi-level pinned a mere 0.12 eV above the midgap ($\psi_s = 0.12$ V), while the passivated $a = 35$ nm NWs were only partially depleted ($r_q \sim 4$ nm) with the Fermi-level 0.36 eV above midgap ($\psi_s = 0.36$ V). Using equation (13), this corresponds to an effective free electron carrier concentration of $n_{\text{eff}} = 4.4 \times 10^{13}$ cm^{-3} for unpassivated NWs and $n_{\text{eff}} = 1.2 \times 10^{17}$ cm^{-3} for passivated NWs, representing a four order of magnitude improvement, thus showing the effectiveness of passivation.

In order to further confirm effective passivation using AlInP shells, TRPL was performed on both passivated and unpassivated samples. Figure 6 shows the PL decay from unpassivated (red curve) and passivated (green curve) NWs. The system time-response, obtained by performing a measurement at the excitation laser wavelength, is also shown as the blue curve. As can be seen, the PL decay from unpassivated NWs (red curve) is very short, with an approximate lifetime of 20 ps. The decay from passivated NWs (green curve) is non-exponential with a tail that extends longer than the ~13 ns between laser pulses, resulting in the strong baseline observed just before the arrival of a laser pulse. Nevertheless, the effective lifetime of the

PL is ∼500 ps, marking a 25 × improvement over the unpassivated sample. This improvement compliments the previously reported 20 × improvement in PL intensity upon AlInP passivation [25].

6. Conclusions

In conclusion, the fabrication and passivation of an ensemble NW device has been successfully demonstrated. During fabrication, sonication was used as a novel method to successfully remove axial AlInP sections, allowing the GaAs NW core to be contacted for *I–V* characterization. Model parameters included the NW radius distribution obtained from SEM, doping density obtained from SIMS, and energy distribution of surface state density estimated from *C–V* measurements. Using reasonable fitting parameters, the NWs were shown to exhibit a 55% decrease in surface state density upon passivation and an impressive four order of magnitude increase in the effective carrier concentration of the characteristic $a = 35$ nm NWs. The thickest 1% of NWs in the ensemble dominated the *I–V* characteristics, which is a behavior that should be common to all ensemble NW devices with a distribution in radius. Finally, passivation was further confirmed by TRPL measurements showing a 25 × improvement of carrier lifetime upon passivation.

Acknowledgments

Financial assistance from the Natural Sciences and Engineering Research Council of Canada, Secretaría de Ciencia y Técnica de la Universidad Nacional de Tucumán (CIUNT 26/E419 and 26/E439) and FONCyT PICT2010–400 (Argentina) are gratefully acknowledged. Assistance with the TEM by Fred Pearson and with the MBE growths by Shahram Tavakoli is gratefully acknowledged.

References

[1] Joyce H J *et al* 2011 *Prog. Quantum Electron.* **35** 23
[2] Lauhon L J, Gudiksen M S and Lieber C M 2004 *Phil. Trans.* A **362** 1247
[3] LaPierre R R 2011 *J. Appl. Phys.* **110** 014310
[4] Putnam M C, Boettcher S W, Kelzenberg M D, Turner-Evans D B, Spurgeon J M, Warren E L, Briggs R M, Lewis N S and Atwater H A 2010 *Energy Environ. Sci.* **3** 1037
[5] Lloyd-Hughes J, Merchant S K E, Fu L, Tan H H, Jagadish C, Castro-Camus E and Johnston M B 2006 *Appl. Phys. Lett.* **89** 232102
[6] Tajik N, Peng Z, Kuyanov P and LaPierre R R 2011 *Nanotechnology* **22** 225402
[7] Sköld N, Karlsson L S, Larsson M W, Pistol M-E, Seifert W, Trägårdh J and Samuelson L 2005 *Nano Lett.* **5** 1943
[8] Noborisaka J, Motohisa J, Hara S and Fukui T 2005 *Appl. Phys. Lett.* **87** 093109
[9] Demichel O, Calvo V, Besson A, Noé P, Salem B, Pauc N, Oehler F, Gentile P and Magnea N 2010 *Nano Lett.* **10** 2323
[10] Parkinson P, Joyce H J, Gao Q, Tan H H, Zhang X, Zou J, Jagadish C, Herz L M and Johnston M B 2009 *Nano Lett.* **9** 3349
[11] Luque A and Hegedus S S 2003 *Handbook of Photovoltaic Science and Engineering* (Chichester, UK: Wiley)
[12] Gu Y, Zhang Y, Li A and Li H 2007 *Mater. Sci. Eng.* B **139** 246
[13] Czaban J A, Thompson D A and LaPierre R R 2009 *Nano Lett.* **9** 148
[14] Chia A C E and LaPierre R R 2011 *Nanotechnology* **22** 245304
[15] Chia A C E, Boulanger J P and LaPierre R R 2013 *Nanotechnology* **24** 045701
[16] Plante M C and LaPierre R R 2008 *Nanotechnology* **19** 495603
[17] Plante M C and LaPierre R R 2008 *J. Cryst. Growth* **310** 356
[18] Chia A C E and LaPierre R R 2012 *J. Appl. Phys.* **112** 063705
[19] Sze S and Ng K K 2006 *Physics of Semiconductor Devices* (Hoboken, NJ: Wiley)
[20] Salehzadeh O, Chen M X, Kavanagh K L and Watkins S P 2011 *Appl. Phys. Lett.* **99** 182102
[21] Caram J, Sandoval C, Tirado M, Comedi D, Czaban J, Thompson D A and LaPierre R R 2010 *Nanotechnology* **21** 134007
[22] Kim T-J and Holloway P H 1997 *Crit. Rev. Solid State Mater. Sci.* **22** 239
[23] Tian B, Zheng X, Kempa T J, Fang Y, Yu N, Yu G, Huang J and Lieber C M 2007 *Nature* **449** 885
[24] Levinshtein M and Shur M 1995 *Handbook Series on Semiconductor Parameters* (Singapore: World Scientific)
[25] Chia A C E, Tirado M, Li Y, Zhao S, Mi Z, Comedi D and LaPierre R R 2012 *J. Appl. Phys.* **111** 094319